Journal of Biomolecular NMR, **17:** 43–54, 2000.
KLUWER/ESCOM
© 2000 *Kluwer Academic Publishers. Printed in the Netherlands.*

A set of HNCO-based experiments for measurement of residual dipolar couplings in ^{15}N, ^{13}C, (^{2}H)-labeled proteins

Perttu Permi[a,*], Paul R. Rosevear[b] & Arto Annila[c]
[a]*Institute of Biotechnology, University of Helsinki, P.O. Box 56, FIN-00014, Helsinki, Finland*
[b]*Department of Molecular Genetics, Biochemistry, and Microbiology, University of Cincinnati, College of Medicine, Cincinnati, OH 45267, U.S.A.*
[c]*VTT Biotechnology, FIN-02044 VTT, Espoo, Finland*

Received 8 November 1999; Accepted 20 March 2000

Key words: calerythrin, cardiac troponin C, HNCO, residual dipolar couplings, spin-state selective filters, TROSY, ubiquitin

Abstract

Several HNCO-based three-dimensional experiments are described for the measurement of $^{13}C'(i-1)$-$^{13}C^{\alpha}(i-1)$, $^{15}N(i)$-$^{13}C'(i-1)$, $^{15}N(i)$-$^{13}C^{\alpha}(i)$, $^{15}N(i)$-$^{13}C^{\alpha}(i-1)$, $^{1}H^{N}(i)$-$^{13}C^{\alpha}(i)$, $^{1}H^{N}(i)$-$^{13}C^{\alpha}(i-1)$, and $^{13}C^{\alpha}(i-1)$-$^{13}C^{\beta}(i-1)$ scalar and dipolar couplings in ^{15}N, ^{13}C, (^{2}H)-labelled protein samples. These pulse sequences produce spin-state edited spectra superficially resembling an HNCO correlation spectrum, allowing accurate and simple measurement of couplings without introducing additional spectral crowding. Scalar and dipolar couplings are measured with good sensitivity from relatively large proteins, as demonstrated with three proteins: cardiac Troponin C, calerythrin and ubiquitin. Measurement of several dipolar couplings between spin-1/2 nuclei using spin-state selective 3D HNCO spectra provides a wealth of structural information.

Introduction

Structural information contained in residual dipolar couplings has rapidly been adopted in biomolecular NMR spectroscopy to determine, refine, and evaluate three-dimensional structures of proteins (Tolman et al., 1995; Tjandra et al., 1997; Bewley et al., 1998; Clore et al., 1998a, b; Cornilescu et al., 1998) and nucleic acids (Hansen et al., 1998). The potential of dipolar couplings for studying molecular dynamics has been demonstrated (Tolman et al., 1997). Relative bond lengths have also been determined from residual dipolar couplings (Ottiger and Bax, 1998). Moreover, dipolar couplings have been used to recognize protein folds (Annila et al., 1999).

Residual dipolar couplings, which arise from anisotropic tumbling of molecules in dilute liquid crystals, are conveniently measured from heteronuclear correlation spectra of ^{13}C and ^{15}N enriched samples. The degree of alignment can be adjusted by varying the concentration of liquid crystal medium (Bax and Tjandra, 1997; Tjandra and Bax, 1997; Hansen et al., 1998), allowing the precise measurement of large $^{1}H^{N}(i)$-$^{15}N(i)$ and $^{1}H^{\alpha}(i)$-$^{13}C^{\alpha}(i)$ as well as intrinsically small $^{1}H^{N}(i)$-$^{13}C'(i-1)$, $^{1}H^{N}(i)$-$^{13}C^{\alpha}(i/i-1)$, $^{13}C'$-$^{13}C^{\alpha}$, $^{13}C^{\alpha}$-$^{13}C^{\beta}$, $^{15}N(i)$-$^{13}C'(i-1)$, $^{15}N(i)$-$^{13}C^{\alpha}(i/i-1)$ dipolar contributions. A number of experiments for obtaining the dipolar and scalar contributions to various couplings between nuclei separated by one, two, three and four bonds have been described (Ottiger et al., 1998; Yang et al., 1998; Cai et al., 1999; Permi et al., 1999a, b; Yang et al., 1999). For example, a two-dimensional experiment determining $H^{N}(i)$-$N(i)$, $H^{N}(i)$-$C'(i-1)$, $N(i)$-$C'(i-1)$ couplings was demonstrated (Wang et al., 1998). Later, to alleviate spectral crowding, a three-dimensional HNCO-based spin-state-selective experiment for measurement of $^{13}C^{\alpha}$-$^{1}H^{\alpha}$ couplings was designed (Yang et al., 1998). Also 'accordion' experiments, to resolve

*To whom correspondence should be addressed. E-mail: Perttu.Permi@helsinki.fi

$H^N(i)$-N(i), N(i)-C′($i-1$), $H^N(i)$-C′($i-1$), C′($i-1$)-$C^\alpha(i-1)$, $H^N(i)$-$C^\alpha(i-1)$ couplings were published (Yang et al., 1999). Very recently, a set of spin-state-selective experiments for measurement of N(i)-C′($i-1$), $H^N(i)$-C′($i-1$), C′($i-1$)-$C^\alpha(i-1)$, N(i)-$C^\alpha(i)$, $H^N(i)$-$C^\alpha(i)$, N(i)-$C^\alpha(i-1)$, and $H^N(i)$-$C^\alpha(i-1)$ couplings from two-dimensional α/β-J ^{15}N-^{1}H correlation spectra, with sensitivity enhancement or TROSY implementations, were devised for SAR by NMR studies (Permi et al., 1999a, b; Permi and Annila, 2000). However, we still see a need for robust experiments that allow automated measurement of couplings in much the same way as main chain resonance assignments are obtained from three-dimensional triple-resonance experiments.

In this paper we describe a suite of three-dimensional triple-resonance experiments, which generate spectra superficially resembling the HNCO spectrum, for the measurement of $^1H^N(i)$-$^{13}C^\alpha(i)$, ^{13}C′($i-1$)-$^{13}C^\alpha(i-1)$, $^{13}C^\alpha(i-1)$-$^{13}C^\beta(i-1)$, $^1H^N(i)$-$^{13}C^\alpha(i-1)$, ^{15}N(i)-^{13}C′($i-1$), ^{15}N(i)-$^{13}C^\alpha(i)$ and ^{15}N(i)-$^{13}C^\alpha(i-1)$ couplings. These particular experiments are designed to circumvent problems associated with signal overlap, partially resolved multiplet components, and transverse relaxation during indirect acquisition times. Together with the HNCO-based experiment for measurement of $^{13}C^\alpha$-$^1H^\alpha$ couplings (Yang et al., 1998) and the spin-state-selective HSQC (Andersson et al., 1998; Ottiger et al., 1998), these experiments form the basis set for convenient measurement of residual dipolar couplings. These dipolar couplings provide useful structural restraints of larger molecular weight non-deuterated, or fully deuterated proteins (Figure 1).

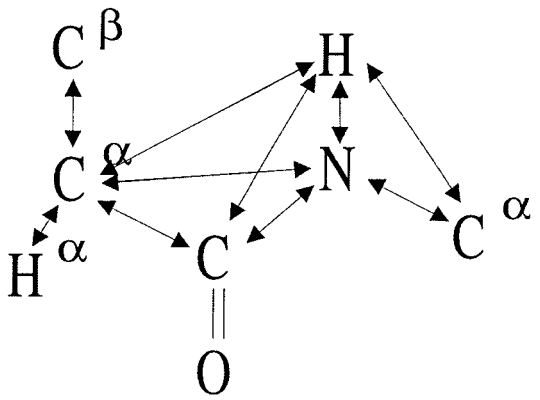

Figure 1. The protein main chain offers a number of one-, two-, and three-bond scalar and dipolar couplings (indicated by arrows) for measurements by spin-state selective two- and three-dimensional NMR experiments. For perdeuterated proteins TROSY variants of the experiments provide the largest gains in sensitivity and resolution. The wealth of directional information contained in dipolar contributions to the couplings allows to define the course of the protein main chain.

Materials and methods

In this study three protein samples were employed, as follows. Measurement of the ^{13}C′-$^{13}C^\alpha$ and ^{13}C′-^{15}N scalar couplings using the proposed HNCO(α/β-C′C^α-*J*) and HNCO(α/β-NC′-*J*) experiments is demonstrated on 1.4 mM uniformly ^{15}N/^{13}C enriched human cardiac Troponin C (cTnC) having a molecular mass of 18 kDa (161 amino acid residues), dissolved in 95/5% H_2O/D_2O in a 270 μl Shigemi microcell, pH 6.5, 40 °C. Corresponding residual dipolar contributions were measured from a 0.3 mM cTnC sample dissolved in dilute liquid crystal composed of filamentous Pf1 phage particles (Hansen et al., 1998). Spectra were recorded on a Varian Unity 600 NMR spectrometer, equipped with a triple-resonance probehead and an actively shielded z-axis gradient system. HNCO(α/β-C′C^α-*J*) spectra for samples in phage solution (water) were acquired with 16 (8) scans per FID with 64, 32, 512 complex points and the corresponding acquisition times of 35.6 ms, 17.8 ms and 64 ms in t_1, t_2, and t_3, respectively. The data were zero-filled to 1024×64×1024 points before Fourier transformation. Data sets of 128, 32, 512 complex points, corresponding to acquisition times of 71.1 ms, 17.8 ms, 64 ms in t_1, t_2, and t_3, respectively, were recorded for the HNCO(α/β-NC′-*J*) spectra of samples in phage solution (water) with 8 (4) scans per FID. The data were zero-filled to 1024×64×1024 points prior to Fourier transformation and phase-shifted squared sine-bell window functions were applied in all dimensions.

Determination of $^1J_{C'C\alpha}$ and $^3J_{H^NC^\alpha}$ couplings using the HNCO(α/β-C′C^α-*J*)-TROSY scheme was tested on 0.7 mM uniformly ^{15}N/^{13}C labeled calerythrin (20 kDa, 176 aa) dissolved in 95/5% H_2O/D_2O in a 250 μl Shigemi microcell, pH 6.0, 45 °C. Spectra were recorded on a Varian Unity INOVA 500 NMR spectrometer, equipped with a triple-resonance probehead and an actively shielded z-axis gradient system, in an interleaved manner with acquisition times of 27.1 ms, 18.8 ms, and 64 ms in t_1, t_2, and t_3, respectively, using 24 transients per FID. The data were zero-filled to 1024×128×1024 points prior to Fourier transformation and phase-shifted squared sine-bell window functions were applied in all dimensions.

Measurement of $^1J_{NC^\alpha}$, $^2J_{NC^\alpha}$, $^2J_{H^NC^\alpha}$, $^3J_{H^NC^\alpha}$, $^1J_{NC'}$ and $^1J_{C^\alpha C^\beta}$ couplings was tested with a 1.0 mM uniformly $^{15}N/^{13}C$ enriched human ubiquitin sample, dissolved in 90/10% H_2O/D_2O in a Wilmad 535PP NMR tube, pH 5.8, 30 °C. The HNCO(α/β-NC$^\alpha$-*J*)-TROSY experiment was recorded using 16 transients per FID with acquisition times of 11.8 ms, 37.6 ms, and 64 ms in t_1, t_2, and t_3, respectively. An accordion value of $\lambda = 3$ was used. The data were zero-filled to 128×1024×1024 points before Fourier transformation and a phase-shifted squared sine-bell window function was applied in all dimensions. The HNCO(C$^\alpha$C$^\beta$-*J*) experiment was recorded using 24 transients per FID with acquisition times of 37.6 ms, 18.8 ms, 64 ms in t_1, t_2, and t_3, respectively. A value of $\lambda = 2$ was used to scale $^1J_{C^\alpha C^\beta}$ with respect to $\omega_{C'}$. The data were post-processed to a 1024×128×1024 matrix prior to Fourier transformation and phase-shifted squared sine-bell window functions were applied in all dimensions. Spectra were recorded on a Varian Unity INOVA 500 NMR spectrometer.

Results and discussion

Method for measuring $^1J_{C'C^\alpha}$ and $^3J_{H^NC^\alpha}$

The HNCO(α/β-C′C$^\alpha$-*J*) pulse sequence for the measurement of one-bond $^{13}C'(i-1)$-$^{13}C^\alpha(i-1)$ and three-bond $^1H^N(i-1)$-$^{13}C^\alpha(i-1)$ couplings in ^{15}N, ^{13}C labeled proteins (Figure 2A) is similar to the HNCO (Kay et al., 1990) and the HN(α/β-COCA-*J*) (Permi et al., 1999b) experiments. The magnetization transfer can be described as follows

$$\begin{aligned} &^1H^N \xrightarrow{J_{NH}} {}^{15}N \xrightarrow{J_{NC'}} {}^{13}C' \xrightarrow{J_{C'C\alpha}} {}^{13}C'(t_1) \\ &\xrightarrow{J_{NC'}} {}^{15}N(t_2) \xrightarrow{J_{NH}} {}^1H^N(t_3) \end{aligned} \qquad (1)$$

where the couplings involved in the transfer steps are indicated above the arrows, and t_{1-3} are acquisition times. The HNCO(α/β-C′C$^\alpha$-*J*) experiment begins with the usual $^1H^N$ to ^{15}N INEPT step, followed immediately by the ^{15}N-$^{13}C'$ transfer step. At point *a*, before the $^{13}C'$ acquisition period, the spin-state-selective filter sensitive to the $^{13}C^\alpha$ spin-state is inserted into the pulse sequence. In the in-phase experiment, the essential state of the spin system (neglecting relaxation) at time point *b*, created by applying 180° pulses on the $^{13}C^\alpha$-frequency (indicated by unfilled wide bars) can be described by the density operator $2N_zC'_y$. The undesired components of magnetization are purged in a manner analogous to the pulsed field gradient z-filter (PFG-z-filter). During t_1 the desired term evolves under carbonyl carbon chemical shift and $^{13}C'$-$^{13}C^\alpha$ coupling as described by the operators $2N_zC'_y \cos(\omega_{C'}t_1) \cos(\pi J_{C'C}\alpha t_1)$ and $4N_zC'_yC^\alpha_z \sin(\omega_{C'}t_1) \sin(\pi J_{C'C^\alpha t_1})$ at time point *c*. Between time points *d* and *e*, the ^{15}N spins are frequency labeled during the t_2 evolution period with simultaneous refocusing of ^{15}N-$^{13}C'$ magnetization and dephasing of ^{15}N-$^1H^N$ coherence. At the end, the magnetization is transferred back to the $^1H^N$ spin by the gradient selected sensitivity-enhanced scheme (Kay et al., 1992; Schleucher et al., 1993).

The second experiment, referred to as the antiphase experiment, is similar to the in-phase experiment except that the 180° pulses (filled wide bars) are applied on $^{13}C^\alpha$-spins, and the $90^\circ_{\phi 5}$ pulse acquires an appropriate 90° phase shift. Hence the spin system, after purging of the undesired magnetization, can be described at time point *b* by the density operator $4N_zC'_yC^\alpha_z$. This term evolves, as in the in-phase experiment, under $^{13}C'$ chemical shift and $^{13}C'$-$^{13}C^\alpha$ coupling Hamiltonians, and at time point *c* it can be described by the density operators $4N_zC'_yC^\alpha_z \cos(\omega_{C'}t_1) \cos(\pi J_{C'C^\alpha t_1})$ and $2N_zC'_y \sin(\omega_{C'}t_1) \sin(\pi J_{C'C^\alpha t_1})$. The ^{15}N chemical shift is again recorded during t_2, which is incorporated into the $^{13}C'$-^{15}N back-transfer step in the usual constant-time manner. Finally, the magnetization is returned to the $^1H^N$ spins, which are detected under composite pulse ^{15}N decoupling. The function of the last 90°($^{13}C'$) pulse is to purge undesired components of magnetization (Permi et al., 1999b).

Post-acquisitional addition and subtraction of the in- and antiphase experiments results in two spectra with correlations at $\omega_{C'}(i-1) + \pi J_{C'C^\alpha}$, $\omega_N(i)$, $\omega_{H^N}(i) + \pi^3 J_{H^NC^\alpha}$ and $\omega_{C'}(i-1) - \pi J_{C'C^\alpha}$, $\omega_N(i)$, $\omega_{H^N}(i) + \pi^3 J_{H^NC^\alpha}$, respectively. This ensures minimum resonance overlap while allowing direct and precise measurement of $^{13}C'$-$^{13}C^\alpha$ coupling constants from the frequency difference in the F_1-dimension of the $|\alpha>$ and $|\beta>$ multiplet components separated into two subspectra. Owing to the finite $^3J_{H^NC^\alpha}$ coupling during the acquisition, a familiar E.COSY pattern emerges and $^3J_{H^NC^\alpha}$ can be measured from the cross-peak displacements in F_3 between two subspectra. However, as the spin-state of $^{13}C^\alpha$ is inverted by the 180°($^{13}C^\alpha$) pulse between the t_1 and t_3 evolution periods, the E.COSY multiplet pattern is opposite to that expected for $^3J_{H^NC^\alpha}$ (Yang et al., 1999).

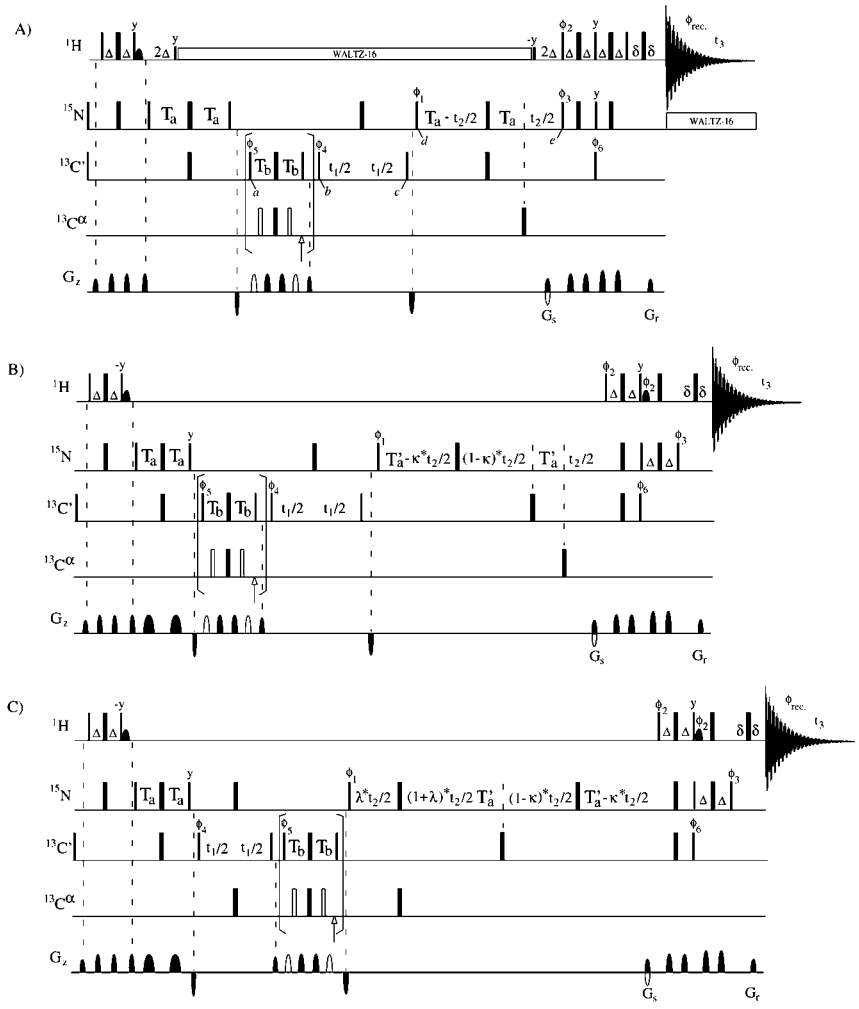

Since the $^{13}C'$-$^{13}C^{\alpha}$ coupling is large (50–55 Hz) and spin-state-selective filtering is utilized, $t_{1,\max}$ can be kept short, i.e. 20–25 ms. Otherwise, in the absence of spin-state editing, a limited acquisition time for $^{1}J_{C'C^{\alpha}}$ coupling would result in $^{13}C'$-$^{13}C^{\alpha}$ doublets which are not resolved to the baseline and the apparent splitting would underestimate the true coupling value. Likewise, experiments with a long time for coupling evolution during t_1 or with an accordion delay will suffer from transverse relaxation.

Figure 3A represents portions of F_1-F_3 planes showing cross peaks from residue E155 of cTnC in the dilute liquid crystal phase obtained after addition and subtraction of the in- and the antiphase data sets, recorded with the HNCO(α/β-$C'C^{\alpha}$-*J*) scheme. The cross peaks in each subspectrum can be picked in the same manner as the conventional HNCO spectra. Traces along the $^{13}C'$ dimension of the two subspectra exhibit no evidence of *J*-crosstalk, as expected. Peak positions are measured precisely from interpolated traces, e.g. by inverse Fourier transformation followed by zero-filling and retransformation. The average chemical shift of the multiplet components coincides, of course, with the carbonyl shift, thus giving it without explicit acquisition of the HNCO spectrum.

For the largest, perdeuterated proteins, it is advantageous to employ transverse relaxation optimized spectroscopy (Pervushin et al., 1997) together with spin-state selection. The corresponding HNCO(α/β-$C'C^{\alpha}$-*J*)-TROSY experiment is illustrated in Figure 2B. The TROSY version is essentially similar to the non-TROSY scheme, except for a few modifications essential for achieving high sensitivity. In this case, the time period for ^{15}N frequency labeling is

Figure 2. A set of three-dimensional experiments for the measurement of scalar and residual dipolar couplings between $^{13}C'(i-1)$-$^{13}C^{\alpha}(i-1)$, $^{15}N(i)$-$^{13}C'(i-1)$, $^{1}H^{N}(i)$-$^{13}C^{\alpha}(i)$, $^{1}H^{N}(i)$-$^{13}C^{\alpha}(i-1)$, $^{15}N(i)$-$^{13}C^{\alpha}(i)$, $^{15}N(i)$-$^{13}C^{\alpha}(i-1)$, and $^{13}C^{\alpha}(i-1)$-$^{13}C^{\beta}(i-1)$ in ^{15}N, ^{13}C, (^{2}H) labeled proteins. Narrow and wide bars correspond to 90° and 180° flip angles, respectively, applied with phase x unless otherwise indicated. All rectangular $^{13}C'$ and ($^{13}C^{\alpha}$) 90° (180°) pulses were applied with a strength of $\Omega/\sqrt{15}$ ($\Omega/\sqrt{3}$), where Ω is the frequency difference between the centers of the $^{13}C'$ and $^{13}C^{\alpha}$ regions. All $^{13}C'$ pulses were applied on-resonance and $^{13}C^{\alpha}$ pulses off-resonance with phase modulation by Ω in pulse sequences A–E. The shaped 180° ($^{13}C^{\alpha}$) pulse denoted by a filled half-ellipse in scheme F had an rSNOB profile (Kupce et al., 1995) with a duration of 245 μs at 500 MHz, generated with the Pbox software package (Kupce and Freeman, 1993). In scheme F, the ^{13}C transmitter was shifted to 43 ppm just before the 90° ϕ_5 pulse and shifted back to 176 ppm immediately before the 90° ϕ_4 pulse. The positions of off-resonance (Bloch–Siegert) compensation pulses are denoted with arrows. The ^{1}H, ^{15}N, $^{13}C'$ and $^{13}C^{\alpha/\beta}$ carrier positions are 4.7 (water), 120 (center of ^{15}N spectral region), 176 (center of $^{13}C'$ spectral region), and 43 ppm (center of aliphatic carbon region), respectively. Frequency discrimination in F_2 was obtained using PEP sensitivity-enhanced gradient selection (Kay et al., 1992; Schleucher et al., 1993) by inverting the sign of the G_s gradient pulse together with the inversion of ϕ_3. In the corresponding TROSY experiments, quadrature detection and TROSY selection in F_2 was obtained by collecting two data sets: (I) $\phi_2 = x$, $\phi_3 = y$; (II) $\phi_2 = -x$, $\phi_3 = -y$; with simultaneous change in the gradient polarity (Weigelt, 1998). Quadrature detection in the $^{13}C'$ dimension was obtained by States-TPPI (Marion et al., 1989) applied to ϕ_4. Pulsed field gradients were inserted as indicated for coherence transfer pathway selection and residual water suppression. For each scheme, the in- and antiphase data were recorded in an interleaved manner and subsequently added and subtracted to separate the multiplet components to two subspectra. Delay durations: $\Delta = \tau = 1/(4J_{HN})$; $T_a = 1/(4J_{NC'})$; $T'_a = T_a - \Delta$; $T_b = 1/(4J_{C'C^{\alpha}})$; δ = gradient + field recovery delay; $\lambda \geq 0$; $0 \leq \kappa \leq T'_a/t_{2,max}$, $0 \leq \mu \leq T_b/t_{1,max}$. Gradient strengths (durations): G_s = 30 G/cm (1.25 ms), G_r = 29.6 G/cm (0.125 ms). The water signal was suppressed by the water flip-back technique to ensure that most of the water magnetization was preserved along the z-axis throughout the pulse sequences and residual transverse magnetization was effectively dephased by the pulsed field gradients (Piotto et al., 1992; Grzesiek and Bax, 1993). (A) 3D-HNCO(α/β-C′C$^{\alpha}$-*J*) pulse sequence for the measurement of scalar and dipolar couplings between $^{1}J_{C'C^{\alpha}}$ and $^{3}J_{H^{N}C^{\alpha}}$, respectively. The phase cycling scheme for the in-phase spectrum is $\phi_1 = x$; $\phi_2 = x$; $\phi_3 = x$; $\phi_4 = 2(x), 2(-x)$; $\phi_5 = x, -x$; $\phi_6 = 4(x), 4(-x)$; $\phi_{rec.} = x, 2(-x), x$. For the antiphase spectrum, ϕ_5 is incremented by 90°. The WALTZ-16 sequence (Shaka et al., 1983) was used to decouple ^{1}H during heteronuclear transfer and ^{15}N during acquisition. (B) 3D-HNCO(α/β-C′C$^{\alpha}$-*J*)-TROSY scheme for determination of $^{1}J_{C'C^{\alpha}}$ and $^{3}J_{H^{N}C^{\alpha}}$. The phase cycling scheme for the in-phase experiment is $\phi_1 = y$; $\phi_4 = 2(x), 2(-x)$; $\phi_5 = x, -x$; $\phi_6 = 4(x), 4(-x)$; $\phi_{rec.} = x, 2(-x), x$. For the antiphase experiment, ϕ_5 is incremented by 90°. (C) 3D-HNCO(α/β-NC$^{\alpha}$-*J*)-TROSY scheme for the measurement of $^{1}J_{NC^{\alpha}}$, $^{2}J_{NC^{\alpha}}$, $^{2}J_{H^{N}C^{\alpha}}$ and $^{3}J_{H^{N}C^{\alpha}}$ couplings. The phase cycling scheme is $\phi_1 = y$; $\phi_4 = 2(x), 2(-x)$; $\phi_5 = x, -x$; $\phi_6 = 4(x), 4(-x)$; $\phi_{rec.} = x, 2(-x)$ x. For the antiphase experiment, ϕ_5 is incremented by 90°. (D) 3D-HNCO(α/β-NC′-*J*) experiment for measuring $^{1}J_{NC'}$ couplings. The phase cycling for $\cos(\pi^{1}J_{NC'}(1+\lambda)t_1)\cos(\omega_{C'}t_1)$ modulated data is $\phi_1 = y$; $\phi_2 = x$; $\phi_3 = x$; $\phi_4 = 2(x), 2(-x)$; $\phi_5 = y, -y$; $\phi_6 = 4(x), 4(-x)$; $\phi_{rec.} = x, 2(-x), x$. For $\sin(\pi^{1}J_{NC'}(1+\lambda)t_1)\sin(\omega_{C'}t_1)$ modulated data, ϕ_5 is incremented by 90°. The WALTZ-16 sequence (Shaka et al., 1983) was used to decouple ^{1}H during heteronuclear transfer and ^{15}N during acquisition. (E) 3D-HNCO(α/β-NC′-*J*)-TROSY scheme for the measurement of $^{1}J_{NC'}$. The phase cycling scheme for $\cos(\pi^{1}J_{NC'}(1+\lambda)t_1)\cos(\omega_{C'}t_1)$ modulated data is $\phi_1 = y$; $\phi_4 = 2(x), 2(-x)$; $\phi_5 = y, -y$; $\phi_6 = 4(x), 4(-x)$; $\phi_{rec.} = x, 2(-x), x$. For $\sin(\pi^{1}J_{NC'}(1+\lambda)t_1)\sin(\omega_{C'}t_1)$ modulated data, ϕ_5 is incremented by 90°. (F) 3D-HNCO(C$^{\alpha}$C$^{\beta}$-*J*)-TROSY scheme for measuring $^{1}J_{C^{\alpha}C^{\beta}}$. Phase cycle: $\phi_1 = y$; $\phi_4 = 2(x), 2(-x)$; $\phi_5 = x, -x$; $\phi_6 = 4(x), 4(-x)$; $\phi_{rec.} = x, 2(-x), x$.

implemented as a semi-constant-time (Logan et al., 1993) (S-CT) TROSY evolution (Permi and Annila, 2000). However, for the optimum sensitivity, the $^{13}C'$-^{15}N back-INEPT step and the first spin-state-selective filter element of the generalized TROSY scheme are concatenated (Salzmann et al., 1999). In addition, the selection for the most slowly relaxing ^{15}N-^{1}H multiplet component is accomplished by the gradient and sensitivity enhanced TROSY implementation (Andersson et al., 1998; Weigelt, 1998). This reduces the phase cycling necessary for the coherence selection while providing excellent water suppression.

The corresponding TROSY cross peaks, after addition and subtraction, appear at $\omega_{C'}(i-1) + \pi^{1}J_{C'C^{\alpha}}$, $\omega_{N}(i) - \pi^{1}J_{NH}$, $\omega_{H^{N}}(i) + \pi^{1}J_{NH} - \pi^{3}J_{H^{N}C_{\alpha}}$ and $\omega_{C'}(i\text{-}1) - \pi^{1}J_{C'C^{\alpha}}$, $\omega_{N}(i) - \pi^{1}J_{NH}$, $\omega_{H^{N}}(i) + \pi^{1}J_{NH} + \pi^{3}J_{H^{N}C^{\alpha}}$, respectively. Therefore, $^{1}J_{C'C^{\alpha}}$ and $^{3}J_{H^{N}C^{\alpha}}$ couplings can be measured analogously to the HNCO(α/β-C′C$^{\alpha}$-*J*) experiment but on the most slowly relaxing ^{15}N-^{1}H multiplet component. A selected F_1-F_3 plane of the HNCO(α/β-C′C$^{\alpha}$-*J*)-TROSY spectrum is exemplified for calerythrin, a calcium binding protein containing 176 residues (Figure 4). A total of 150 out of 162 possible $^{1}J_{C'C^{\alpha}}$ scalar couplings could be measured from calerythrin by using the proposed HNCO(α/β-C′C$^{\alpha}$-*J*)-TROSY scheme.

Method for measuring $^{1}J_{NC^{\alpha}}$, $^{2}J_{NC^{\alpha}}$, $^{2}J_{H^{N}C^{\alpha}}$, *and* $^{3}J_{H^{N}C^{\alpha}}$ *couplings*

The three-dimensional HNCO(α/β-NC$^{\alpha}$-*J*)-TROSY experiment for the simultaneous measurement of $^{1}J_{NC^{\alpha}}$, $^{2}J_{NC^{\alpha}}$, $^{2}J_{H^{N}C^{\alpha}}$ and $^{3}J_{H^{N}C^{\alpha}}$ couplings in protonated or perdeuterated proteins is presented in Figure 2C. The pulse sequence mostly resembles the HNCO(α/β-C′C$^{\alpha}$-*J*)-TROSY scheme, but differs as follows. Firstly, the 180°($^{13}C^{\alpha}$) is applied in the middle of the t_1 period to decouple the $^{13}C^{\alpha}$ spin. Additionally, the spin-state-selective filter is now placed between the t_1 and t_2 evolution periods. Thus, analogous to the HNCO(α/β-C′C$^{\alpha}$-*J*)-TROSY experiment,

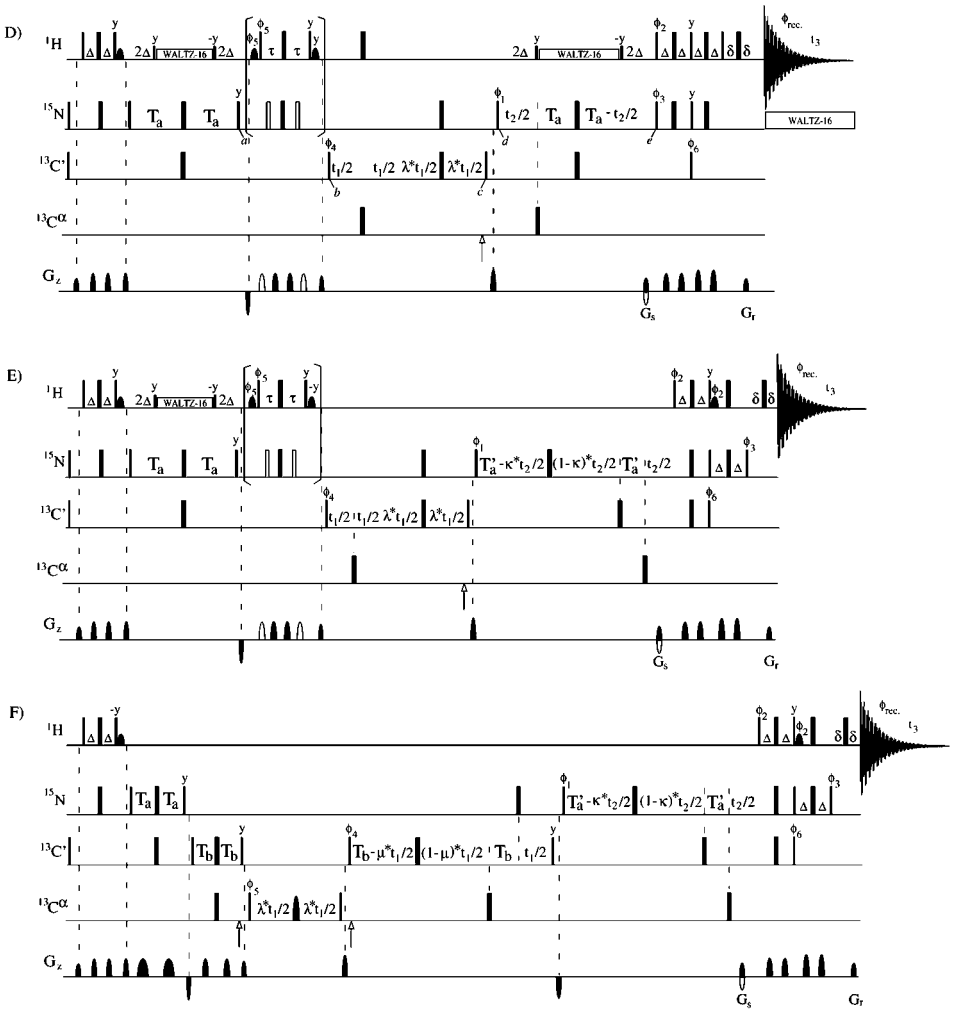

Figure 2. (continued).

the $^{13}C^{\alpha}$ spin-state is edited to create $4H_z^N N_z C'_z$ and $8H_z^N N_z C'_z C_z^{\alpha}$ coherence for the in- and antiphase experiments before t_2, respectively. During the ensuing t_2 period, which we implement again in an S-CT TROSY manner, the ^{15}N is allowed to couple with both intra- and interresidual $^{13}C^{\alpha}$ spins. Due to the relatively small value of the $^1J_{NC^{\alpha}}$ coupling (9–12 Hz), we utilize accordion spectroscopy (Bodenhausen and Ernst, 1981) style *J*-multiplication to scale up $^1J_{NC^{\alpha}}$ and $^2J_{NC^{\alpha}}$. This can be accomplished by inserting an additional spin-echo period for the $J_{NC}\alpha$ evolution. After adequate data processing, cross peaks are observed at $\omega_{C'}(i-1)$, $\omega_N(i) - \pi^1 J_{NH} + (1+\lambda)\pi^2 J_{NC^{\alpha}} \pm (1+\lambda)\pi^1 J_{NC^{\alpha}}$, $\omega_{H^N}(i) + \pi^1 J_{NH} + \pi^3 J_{H^N C^{\alpha}} \pm \pi^2 J_{H^N C^{\alpha}}$ and $\omega_{C'}(i-1)$, $\omega_N(i) - \pi^1 J_{NH} - (1+\lambda)\pi^2 J_{NC^{\alpha}} \pm (1+\lambda)\pi^1 J_{NC^{\alpha}}$, $\omega_{H^N}(i) + \pi^1 J_{NH} - \pi^3 J_{H^N C^{\alpha}} \pm \pi^2 J_{H^N C^{\alpha}}$, for the two three-dimensional subspectra, respectively. As noted above, the $^1J_{NC^{\alpha}}$ and $^2J_{NC^{\alpha}}$ are multiplied by $1+\lambda$, and consequently $^1J_{NC^{\alpha}}$ can be extracted from the apparent splitting with division by $1+\lambda$, whereas the $^2J_{NC^{\alpha}}$ is invariably resolved by the spin-state selection. The corresponding $^2J_{H^N C^{\alpha}}$ and $^3J_{H^N C^{\alpha}}$ couplings can be measured in F_3. Use of concomitant scaling of $^1J_{NC^{\alpha}}$ (and $^2J_{NC^{\alpha}}$) assumes, however, that the relaxation rate of the TROSY component is not significantly larger than $^1J_{NC^{\alpha}}$. In favorable cases this postulation is fulfilled even for larger proteins. For example, Kay and co-workers have estimated a transverse relaxation time of ∼70 ms for the ^{15}N TROSY component in the perdeuterated protein MBP containing 370 residues (Yang et al., 1999). For smaller proteins this relaxation condition is easily

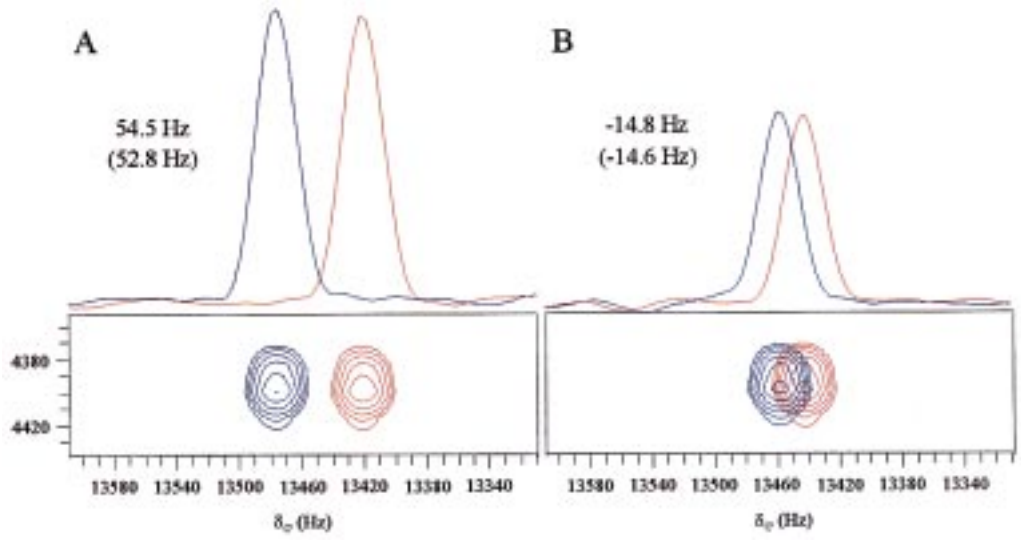

Figure 3. Representative F_1-F_3 plane of E155 of the HNCO(α/β-C′C$^{\alpha}$-*J*) (A) and the HNCO(α/β-NC′-*J*) (B) spectra recorded at 600 MHz on cTnC in the liquid crystal phase. The upfield (red) and downfield (blue) multiplet components of the corresponding ^{13}C′-^{15}N and ^{13}C′-^{13}C$^{\alpha}$ doublets obtained by post-acquisitional summation and subtraction of the in-phase and antiphase data sets are overlaid. The measured couplings in the anisotropic medium (in water) are indicated in the spectra, showing dipolar contributions to the ^{13}C′-^{13}C$^{\alpha}$ and ^{13}C′-^{15}N splitting of 1.7 Hz and −0.2 Hz, respectively. 142 ^{13}C′-^{13}C$^{\alpha}$ and 140 ^{13}C′-^{15}N dipolar couplings were measured from the HNCO(α/β-C′C$^{\alpha}$-*J*) and the HNCO(α/β-NC′-*J*) spectra, respectively.

met, as demonstrated with the data shown in Figure 5 recorded from ubiquitin using the pulse scheme in Figure 2C.

The accurate measurement of coupling constants from spin-state edited spectra assumes that there is no significant *J*-crosstalk in either subspectrum. There are several factors possibly degrading subspectral editing, i.e. *J*-mismatch, cross-correlated relaxation, differential relaxation and pulse imperfections. Their influence on the measurement of couplings and elimination of these artefacts have been discussed (Meissner and Sørensen, 1998; Ottiger et al., 1998; Permi et al., 1999a, b). As we have shown previously, the spin-state-selective filter tuned to the $^{1}J_{C'C^{\alpha}} = 55$ Hz coupling is largely insensitive to the *J*-mismatch in the frequency range from 45 to 65 Hz (Permi et al., 1999b). In the anisotropic medium, the dipolar contribution to the ^{13}C′-^{13}C$^{\alpha}$ coupling can be estimated to be ∼6 Hz at maximum which, for example, relates to a maximal 25–30 Hz dipolar contribution for the one-bond ^{15}N-^{1}H coupling. Therefore, it is unlikely that the *J*-mismatch would cause *J*-crosstalk. Effects of the cross-correlated relaxation between the ^{13}C′ chemical shift anisotropy (CSA) and the ^{13}C′-^{13}C$^{\alpha}$ dipole–dipole (DD) relaxation mechanisms (Goldman, 1984) are also taken into account by averaging relaxation for the ^{13}C$^{\alpha}$ spin-states during the filter element (Andersson et al., 1998b). If it is necessary, the *J*-crosstalk artefacts can be eliminated by scaling the in- or antiphase spectrum prior to Fourier transformation, which is equivalent to taking an appropriate linear combination of the two subspectra (Ottiger et al., 1998; Sørensen et al., 1999). Cross correlation between the ^{13}C′ and remote carbon spins during the t_1 evolution period may, in principle, influence peak positions in the ^{13}C′ dimension in the HNCO(α/β-C′C$^{\alpha}$-*J*) experiments. Owing to the different linewidths of an unresolved ^{13}C′-^{13}C^{r} (*r* stands for a remote ^{13}C spin) doublet arising from the small ^{13}C′-^{13}C^{r} coupling, the lines of ^{13}C′-^{13}C$^{\alpha}$ doublet components may be distorted. While estimation of the size of the cross correlation is non-trivial, these effects remain small due to the short t_1 time and are suppressed by apodization required to avoid truncation effects in F_1.

Method for measuring $^{1}J_{NC'}$

The HNCO(α/β-NC′-*J*) pulse sequence for the measurement of ^{15}N(*i*)-^{13}C′(*i* − 1) coupling (Figure 2D) is similar to the HNCO(α/β-C′C$^{\alpha}$-*J*) experiment, but the α/β-filter is tuned to a ^{15}N-^{1}H coupling. The flow of

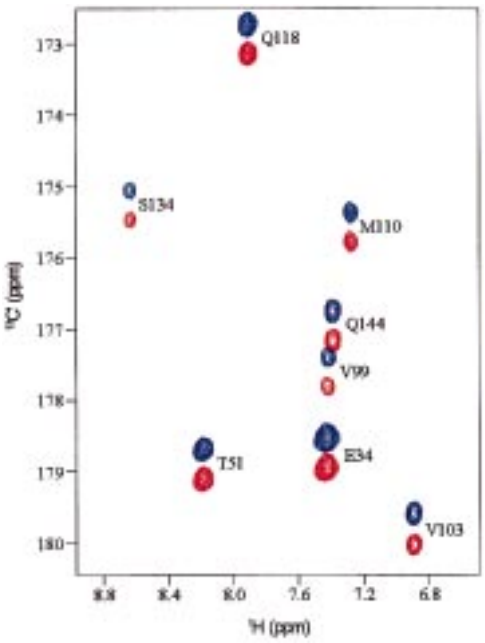

Figure 4. Representative region of the HNCO(α/β-C′C$^{\alpha}$-*J*)-TROSY spectrum, recorded from 0.7 mM U-(^{15}N, ^{13}C) calerythrin. The $^{1}J_{C'C^{\alpha}}$ can be measured from the cross-peak displacement in the F_1-dimension between two subspectra, which are overlaid. The finite $^{3}J_{H^{N}C^{\alpha}}$ coupling is obtained from cross-peak displacement in the F_3-dimension. Upfield (blue) and downfield (red) multiplet components, processed to separate subspectra, are shown superimposed for E34, T51, V99, V103, M110, Q118, S134, and Q144 at the cross-section of E34 ^{15}N.

coherence can be described schematically as follows:

$$^{1}H^{N} \xrightarrow{J_{NH}} {}^{15}N \xrightarrow{J_{NC'}} {}^{1}H^{N} \xrightarrow{J_{NH}} {}^{13}C'(t_1) \xrightarrow{J_{NC'}} {}^{15}N(t_2) \xrightarrow{J_{NH}} {}^{1}H^{N}(t_3) \quad (2)$$

Initially, the ^{1}H^{N} magnetization is transferred to its directly bonded amide nitrogen and then from ^{15}N to the preceding ^{13}C′. In order to improve the sensitivity of the experiment, a composite pulse decoupling is applied on proton during certain parts of the 2∗T$_a$ delays. The spin-state-selective filter element is inserted into the pulse sequence before the t_1 evolution period (time points *a*–*b*). In the in-phase experiment, only the 180° (^{15}N) pulses marked with unfilled wide bars are employed, resulting in an effective decoupling of $^{1}J_{NH}$. Thus, the magnetization at time point *b* can be described by the density operator $4H_z^N N_z C'_y$, which is allowed to modulate under the ^{13}C′ chemical shift and the ^{13}C′($i-1$)-^{15}N(i) coupling during t_1. After frequency labeling in t_1, the cosine modulated magnetization is transferred back to the amide nitrogen, which is frequency labeled during the following constant time t_2 evolution period (time points *d*–*e*). Finally, the gradient selected sensitivity enhanced scheme transfers magnetization back onto the amide proton. In the corresponding antiphase experiment, the heteronuclear coupling between ^{1}H^{N} and ^{15}N is refocused by applying a 180°(^{15}N) pulse, indicated by the filled wide bar. The desired magnetization component before t_1 is described by the density operator $2H_z^N C'_y$ (time point *b*), which evolves to $4H_z^N N_z C'_y \sin(\omega_{C'} t_1) \sin(\pi J_{NC'}(1+\lambda)t_1)$ (time point *c*). Subsequently, the nitrogen chemical shift is detected during t_2 and the amide proton chemical shift during t_3. The last pulse on ^{13}C′ serves to purge undesired components of magnetization. In summary, by addition and subtraction of these two data sets, the HNCO-type correlations arise at $\omega_{C'}(i-1) + (1+\lambda)\pi^{1}J_{NC'}$, $\omega_N(i)$, $\omega_{H^N}(i)$ and $\omega_{C'}(i-1) - (1+\lambda)\pi^{1}J_{NC'}$, $\omega_N(i)$, $\omega_{H^N}(i)$. Again, the frequency difference in the F_1 dimension between the cross-peak placements in the two subspectra will directly yield the $^{1}J_{NC'}$ couplings. Figure 3B shows a portion of the F_1-F_3 plane representing cross peaks from residue E155 of cTnC in the dilute liquid crystal phase obtained after addition and subtraction of cosine and sine modulated data sets, recorded with the HNCO(α/β-NC′-*J*) scheme.

The corresponding TROSY implementation of the HNCO(α/β-NC′-*J*) experiment is shown in Figure 2E. The latter part of the HNCO(α/β-NC′-*J*)-TROSY scheme is identical to the HNCO(α/β-C′C$^{\alpha}$-*J*)-TROSY sequence. However, it is implicit that when the $^{1}J_{NH}$ coupling is used to edit the ^{15}N spin-state, the TROSY implementation will improve the sensitivity only during the S-CT t_2 evolution period and acquisition. The 180° (^{1}H) pulse during the filter will interchange fast and slowly relaxing multiplet components and a small improvement in the sensitivity was obtained using the coherent proton decoupling during the ^{15}N-^{13}C′ out-transfer step. Note that in this case, the ^{15}N steady-state magnetization cannot be added to $H_z^N N_y$ coherence for enhanced sensitivity. Eventually, after addition and subtraction of the in- and antiphase data sets, cross peaks appear at $\omega_{C'}(i-1) + (1+\lambda)\pi^{1}J_{NC'}$, $\omega_N(i) - \pi^{1}J_{NH}$, $\omega_{H^N}(i) + \pi^{1}J_{NH}$ and $\omega_{C'}(i-1) - (1+\lambda)\pi^{1}J_{NC'}$, $\omega_N(i) - \pi^{1}J_{NH}$, $\omega_{H^N}(i) + \pi^{1}J_{NH}$.

The separation of α- and β-states in the HNCO(α/β-NC′-*J*) experiments is based on the large one-bond scalar $^{1}J_{NH}$ coupling, which is nearly uniform (93 ± 2 Hz). Tolerance against the *J*-mismatch is excellent also in the anisotropic phase, where deviations up to 20–30 Hz from the scalar 93 Hz can

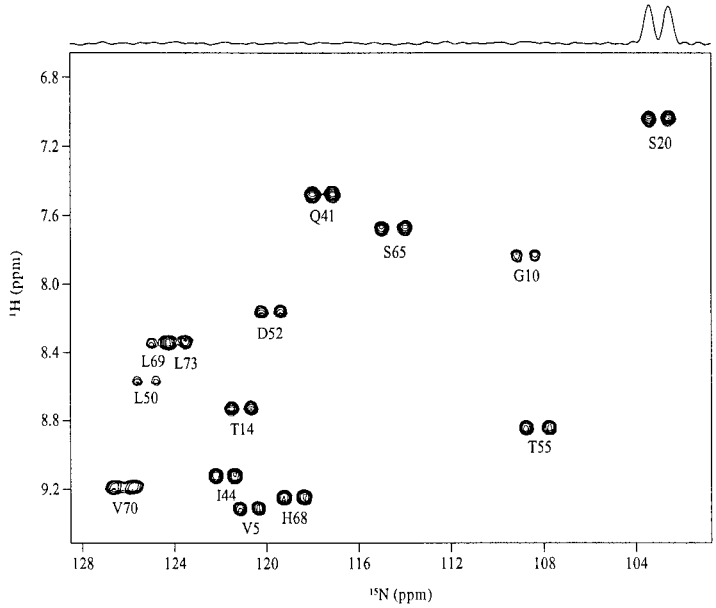

Figure 5. Expansion of HNCO(α/β-NC$^{\alpha}$-*J*)-TROSY subspectrum recorded from ubiquitin. The spectrum contains, in the in-phase multiplet components, the intraresidue $^1J_{NC^{\alpha}}$ and $^2J_{H^NC^{\alpha}}$ couplings along the ^{15}N and ^{1}H dimensions, respectively. The F_2-F_3 expansion was taken at the ^{13}C′ chemical shift of P19. The one-dimensional trace through S20 shows a clearly resolved doublet split by the $^1J_{NC^{\alpha}}$ coupling, multiplied with a factor of 4 ($\lambda = 3$).

be expected. The $^1J_{NC'}$ coupling constants are between 14–16 Hz (Delaglio et al., 1991) for the majority of residues in proteins. Dipolar contributions are small, owing to the small product of the gyromagnetic ratios of ^{15}N and ^{13}C, and deviations up to ± 3 Hz can be expected (assuming a dipolar contribution for the one-bond NH coupling to be ∼25 Hz). It is then necessary to acquire t_1 close to 60 ms. If desirable, accordion-type spectroscopy to follow the coupling independently of the chemical shift evolution can be used to reduce the number of increments during t_1 in a manner similar to the HNCO(α/β-NC$^{\alpha}$-*J*)-TROSY experiment. Thus, the limiting factor for the HNCO(α/β-NC′-*J*) experiments at high fields is the transverse relaxation of the ^{13}C′ spin which is dominated by the CSA relaxation mechanism. The ^{13}C′ linewidth increases quite rapidly with increasing magnetic field. Transverse relaxation for the ^{13}C′ spin in the protein backbone can be approximated by $T_{2C'} \sim 1/\tau_c\,(3/4 + B^2/150)$ s, where τ_c is the isotropic molecular rotational correlation time given in nanoseconds, and *B* is the magnetic field strength in tesla (Hu and Bax, 1997). For this reason the HNCO(α/β-NC′-*J*) experiment is best carried out at field strengths of ≤ 600 MHz proton frequency.

In order to evaluate the effect of crosstalk on the measured coupling constant in the case of partially overlapping ^{15}N-^{13}C′ doublet components, we took an array of linear combinations of the in- and antiphase HNCO(α/β-NC′-*J*) spectra. Thus, crosstalk was created artificially in varying amounts and its influence on the principal peak frequency was investigated (Figure 6). Our results imply that even a very large amount, up to 40%, of crosstalk will not markedly affect the peak placement, i.e. ∼0.1–0.2 Hz, corresponding to 0.2–0.4 Hz in the measured coupling constant. However, the amount of *J*-crosstalk arising from the *J*-mismatch or differential relaxation is small, ≤ ±10% in practice, and therefore the imprecision in peak placement will fall below 0.1 Hz. The obvious implication is that the error arising from a small *J*-crosstalk is on the order of the measurement accuracy, which is most likely dictated by other sources of error that will distort the lineshape in general. In the case of broad lines, in particular, the in-phase crosstalk artefacts are more difficult to detect but affect the apparent splitting less than the antiphase crosstalk artefacts. It should be noted that the error in the measured coupling constant increases with linewidth. Therefore it may be worthwhile to scale up the measured coupling by accordion style spectroscopy. Additional benefit

from this approach is the decreased measurement error, since the apparent splitting is divided by a factor $(1+\lambda)$ to obtain actual coupling.

Method for measuring $^1J_{C^\alpha C^\beta}$

The HNCO($C^\alpha C^\beta$-*J*)-TROSY pulse sequence (Figure 2F) is suitable for measuring $^1J_{C^\alpha C^\beta}$ both in protonated and perdeuterated samples. In this approach we first transfer $^1H^N$ magnetization to its interresidual $^{13}C^\alpha$ spin via ^{15}N and $^{13}C'$ spins utilizing standard building blocks for coherence transfer. During the following t_1 evolution period, the $^1J_{C^\alpha C^\beta}$ coupling is detected while the evolutions of $^{13}C^\alpha$ chemical shift and other couplings are refocused by inserting a 180° ($^{13}C^\alpha$) pulse in the middle of the $\lambda * t_1$ period. The desired magnetization is in the form $8H_z^N N_z C'_z C^\alpha_y \cos(\pi {}^1J_{C^\alpha C^\beta} \lambda t_1)$ at the end of the t_1 period, and is subsequently transferred to $8H_z^N N_z C'_y C^\alpha_z \cos(\pi {}^1J_{C^\alpha C^\beta} \lambda t_1)$ coherence. The chemical shift of $^{13}C'$ is frequency labeled during t_1, which is implemented as a semi-constant-time to obtain sufficient resolution in F_1. The ^{15}N chemical shift is detected during an S-CT TROSY evolution period, as shown for the TROSY experiments above. Finally, the magnetization is transferred back to the $^1H^N$ spin using the gradient and sensitivity enhanced TROSY scheme. Correlations occur at frequencies $\omega_{C'}(i-1) \pm \lambda\pi {}^1J_{C^\alpha C^\beta}$, $\omega_N(i) - \pi {}^1J_{NH}$, $\omega_{H^N}(i) + \pi {}^1J_{NH}$. Hence, the $^1J_{C^\alpha C^\beta}$ is determined from the displacement of multiplet components in F_1. The separation of $^{13}C^\alpha$-$^{13}C^\beta$ multiplet components into different subspectra is difficult owing to the overlapping $^{13}C^\alpha$-$^{13}C^\beta$ frequencies, therefore editing with respect to spin-states is not employed for the measurement of $^1J_{C^\alpha C^\beta}$. A representative F_1-F_3 plane from ubiquitin is shown in Figure 7. Owing to the favorable $^{13}C^\alpha$ relaxation time found also in protonated ubiquitin, the measured $^1J_{C^\alpha C^\beta}$ couplings were scaled up by a factor of 2 with respect to the $^{13}C'$ chemical shift. This is not feasible for the larger protonated proteins due to rapid transverse relaxation of $^{13}C^\alpha$. It is obvious that in protonated samples the $^1H^\alpha$ spin could be decoupled from $^{13}C^\alpha$, without compromising TROSY enhancement, by a semi-selective decoupling of $^1H^\alpha$ spins during the t_1 period.

An interesting detail concerns the selective 180° pulse employed for both the $^{13}C^\alpha$ and the $^{13}C^\beta$ spin during the $\lambda * t_1$ period. The purpose of this pulse is to refocus the $^{13}C^\alpha$ chemical shift evolution and to invert the $^{13}C^\beta$ spins. A usual rectangular 180° pulse applied at ~43 ppm is not capable of inverting $^{13}C^\beta$ spins properly throughout the $^{13}C^\beta$ chemical shift range. For this reason we have used a shaped rSNOB profile (Kupce et al., 1995) for the selective 180° pulse to guarantee inversion of $^{13}C^\beta$ spins with simultaneous refocusing of $^{13}C^\alpha$ spins. For perdeuterated samples, where the transverse relaxation time of the $^{13}C^\alpha$ spin is considerably longer than that of the $^{13}C'$ spin, it may be advantageous to record both the chemical shift and $^1J_{C^\alpha C^\beta}$ coupling evolution on the $^{13}C^\alpha$ spin. Of course, a small modification in the pulse sequence is needed to employ deuterium decoupling during which the $^{13}C^\alpha$ spin is in the transverse plane, i.e. for the $\lambda * t_1$ period.

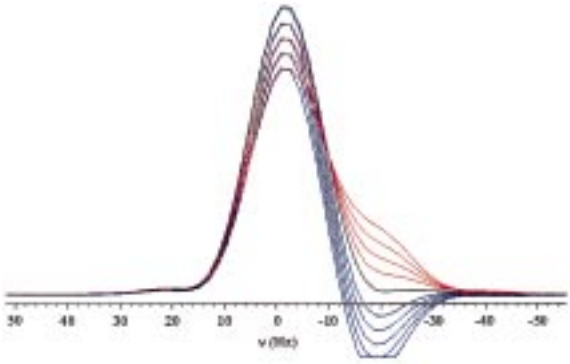

Figure 6. Illustration of different amounts of *J*-crosstalk affecting the apparent peak placement in the HNCO(α/β-NC′-*J*) spectrum. The 1D slices from G140, transformed with varying amounts of *J*-crosstalk obtained by scaling the in- and antiphase spectrum with respect to each other, are overlaid. The spectrum with the highest amplitude is virtually free from crosstalk. The 1D slices showing *J*-crosstalk, either positive (red) or negative (blue) crosstalk, were generated by scaling the in- and antiphase spectra by 0, −3, ±10, ±20, ±30, ±40% with respect to each other. The data were zero-filled to 2K×64×1K points before Fourier transformation. A phase-shifted squared sine-bell window function was applied in all dimensions.

Conclusions

We have described a set of three-dimensional spin-state-selective HNCO-based experiments for measurements of scalar and dipolar couplings in larger proteins. Couplings of interest are resolved efficiently and accurately by spin-state-selective filters. The experiments described are also applicable to perdeuterated samples and in large molecular weight systems orientation of the $^{13}C'$-$^{13}C^\alpha$ and ^{15}N-$^{13}C'$ internuclear bond vectors can be determined. Measurement of several dipolar couplings with presented pulse sequences will define more precisely the course of the protein backbone and the opening directions of side chains.

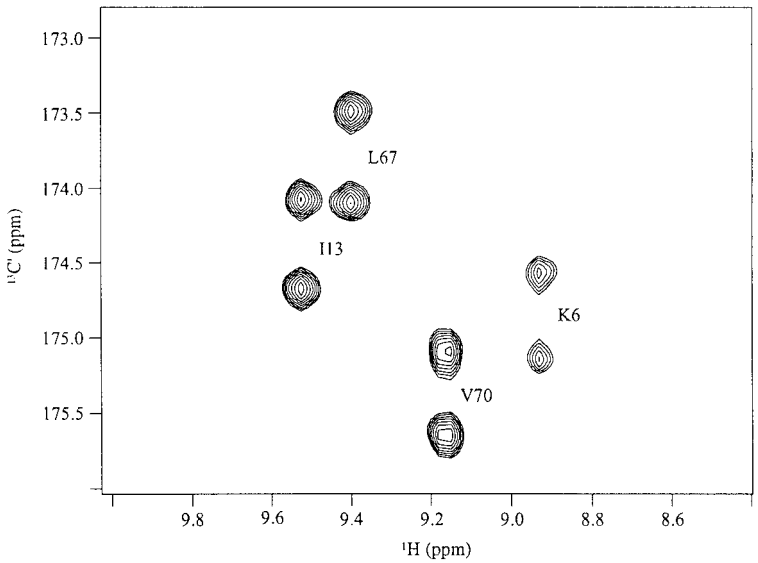

Figure 7. Representative portion of the HNCO(C^{α} C^{β}-*J*)-TROSY spectrum of ubiquitin. Cross peaks are shown for K6, I13, L67, and V70 residues at the ^{15}N cross-section of I13. The cross peaks are split by apparent $2*{}^{1}J_{C^{\alpha}C^{\beta}}$ in the F_1-dimension ($\lambda = 2$).

A large number of residual dipolar couplings in non-redundant directions will allow the principal components of the alignment tensor to be estimated precisely (Clore et al., 1999a, b) for the normalized frequency distribution or to be obtained from singular value decomposition (Moltke and Grzesiek, 1999). It is often problematic to obtain a thorough sampling of directions from only NH bond vectors, which tend to group for α-helical proteins in particular. In β-sheet structures the strands are often twisted and result in a larger dispersion of dipolar couplings. The use of multiple dipolar couplings per residue effectively smoothens the non-linear dependence of each individual dipolar coupling with respect to the polar angles. Protein structure determination and refinement will benefit from the constructive use of several residual dipolar couplings available from the 3D HNCO and 2D ^{15}N-^{1}H correlation spectra. These experiments provide data as soon as sequential main chain assignment is accomplished, to reveal structural homology and major conformational changes – the essence of structural biology.

Acknowledgements

This work has been supported by the Academy of Finland and by grant AR44324 (to P.R.R.) from the National Institutes of Health. Helena Aitio is acknowledged for providing the assignments of calerythrin.

References

Andersson, P., Annila, A. and Otting, G. (1998a) *J. Magn. Reson.*, **133**, 364–367.
Andersson, P., Weigelt, J. and Otting, G. (1998b) *J. Biomol. NMR*, **12**, 435–441.
Annila, A., Aitio, H., Thulin, E. and Drakenberg, T. (1999) *J. Biomol. NMR*, **14**, 223–230.
Bax, A. and Tjandra, N. (1997) *J. Biomol. NMR*, **10**, 289–292.
Bewley, C.A., Gustafson, K.R., Boyd, M.R., Covell, D.G., Bax, A., Clore, G.M. and Gronenborn, A.M. (1998) *Nat. Struct. Biol.*, **5**, 571–578.
Bodenhausen, G. and Ernst, R.R. (1981) *J. Magn. Reson.*, **45**, 367–373.
Cai, M., Wang, H., Olejniczak, E.T., Meadows, R.P., Gunasekera, A.H., Xu, N. and Fesik, S.W. (1999) *J. Magn. Reson.*, **139**, 451–453.
Clore, G.M., Gronenborn, A.M. and Tjandra, N. (1998a) *J. Magn. Reson.*, **131**, 159–162.
Clore, G.M., Gronenborn, A.M. and Bax, A. (1998b) *J. Magn. Reson.*, **133**, 216–221.
Cornilescu, G., Marquardt, J.L., Ottiger, M. and Bax, A. (1998) *J. Am. Chem. Soc.*, **120**, 6836–6837.
Delaglio, F., Torchia, D.A. and Bax, A. (1991) *J. Biomol. NMR*, **1**, 439–446.
Goldman, M. (1984) *J. Magn. Reson.*, **60**, 437–452.
Grzesiek, S. and Bax, A. (1993) *J. Am. Chem. Soc.*, **115**, 12593–12594.
Hansen, M.R., Mueller, L. and Pardi, A. (1998) *Nat. Struct. Biol.*, **5**, 1065–1074.
Hu, J.-S. and Bax, A. (1997) *J. Am. Chem. Soc.*, **119**, 6360–6368.
Kay, L.E., Ikura, M., Tschudin, R. and Bax, A. (1990) *J. Magn. Reson.*, **89**, 496–514.
Kay, L.E., Keifer, P. and Saarinen, T. (1992) *J. Am. Chem. Soc.*, **114**, 10663–10665.
Kupce, E. and Freeman, R. (1993) *J. Magn. Reson.*, **A105**, 234–239.

Kupce, E., Boyd, J. and Campbell, I.D. (1995) *J. Magn. Reson.*, **B106**, 300–304.
Logan, T.M., Olejniczak, E.T., Xu, R.X. and Fesik, S.W. (1993) *J. Biomol. NMR*, **3**, 225–231.
Marion, D., Ikura, M., Tschudin, R. and Bax, A. (1989) *J. Magn. Reson.*, **85**, 393–399.
Meissner, A., Duus, J.Ø. and Sørensen, O.W. (1997) *J. Biomol. NMR*, **10**, 89–94.
Meissner, A., Schulte-Herbrüggen, T. and Sørensen, O.W. (1998) *J. Am. Chem. Soc.*, **120**, 7989–7990.
Moltke, S. and Grzesiek, S. (1999) *J. Biomol. NMR*, **15**, 77–82.
Ottiger, M. and Bax, A. (1998) *J. Am. Chem. Soc.*, **120**, 12334–12341.
Ottiger, M., Delaglio, F. and Bax, A. (1998) *J. Magn. Reson.*, **131**, 373–378.
Permi, P., Heikkinen, S., Kilpeläinen, I. and Annila, A. (1999a) *J. Magn. Reson.*, **140**, 32–40.
Permi, P., Sorsa, T., Kilpeläinen, I. and Annila, A. (1999b) *J. Magn. Reson.*, **141**, 44–51.
Permi, P. and Annila, A. (2000) *J. Biomol. NMR*, **16**, 221–227.
Pervushin, K., Riek, R., Wider, G. and Wüthrich, K. (1997) *Proc. Natl. Acad. Sci. USA*, **94**, 12366–12371.
Piotto, M., Sauder, V. and Sklenar, V.J. (1992) *J. Biomol. NMR*, **2**, 661–665.
Salzmann, M., Wider, G., Pervushin, K. and Wüthrich, K. (1999) *J. Biomol. NMR*, **15**, 181–184.
Schleucher, J., Sattler, M. and Griesinger, C. (1993) *Angew. Chem. Int. Ed. Engl.*, **32**, 1489–1491.
Shaka, A.J., Keeler, J., Frenkiel, T. and Freeman, R. (1983) *J. Magn. Reson.*, **52**, 335–338.
Sørensen, M.D., Meissner, A. and Sørensen, O.W. (1999) *J. Magn. Reson.*, **137**, 237–242.
Tjandra, N., Szabo, A. and Bax, A. (1996) *J. Am. Chem. Soc.*, **118**, 6986–6991.
Tjandra, N., Omichinski, J.G., Gronenborn, A.M., Clore, G.M. and Bax, A. (1997) *Nat. Struct. Biol.*, **4**, 732–738.
Tjandra, N. and Bax, A. (1997) *Science*, **278**, 1111–1114.
Tolman, J.R., Flanagan, J.M., Kennedy, M.A. and Prestegard, J.H. (1995) *Proc. Natl. Acad. Sci. USA*, **92**, 9279–9283.
Tolman, J.R., Flanagan, J.M., Kennedy, M.A. and Prestegard, J.H. (1995) *Nat. Struct. Biol.*, **4**, 292–297.
Wang, Y.-X., Marquardt, J.L., Wingfield, P., Stahl, S. J., Lee-Huang, S., Torchia, D. and Bax, A. (1998) *J. Am. Chem. Soc.*, **120**, 7385–7386.
Weigelt, J. (1998) *J. Am. Chem. Soc.*, **120**, 10778–10779.
Yang, D., Tolman, J.R., Goto, N.K. and Kay, L.E. (1998) *J. Biomol. NMR*, **12**, 325–332.
Yang, D., Venters, R.A., Mueller, G.A., Choy, W.Y. and Kay, L.E. (1999) *J. Biomol. NMR*, **14**, 333–343.